Analysis of analogue models by helical X-ray computed tomography

G. SCHREURS[1], R. HÄNNI[1], M. PANIEN[1] & P. VOCK[2]

[1] *Institute of Geological Sciences, University of Bern, Baltzerstrasse 1 CH-3012 Bern, Switzerland (e-mail: schreurs@geo.unibe.ch)*

[2] *Institute of Diagnostic Radiology, Inselspital, CH-3010 Bern, Switzerland*

Abstract: The aim of analogue model experiments in geology is to simulate structures in nature under specific imposed boundary conditions using materials whose rheological properties are similar to those of rocks in nature. In the late 1980s, X-ray computed tomography (CT) was first applied to the analysis of such models. In early studies only a limited number of cross-sectional slices could be recorded because of the time involved in CT data acquisition, the long cooling periods for the X-ray source and computational capacity. Technological improvements presently allow an almost unlimited number of closely spaced serial cross-sections to be acquired and calculated. Computer visualization software allows a full 3D analysis of every recorded stage. Such analyses are especially valuable when trying to understand complex geological structures, commonly with lateral changes in 3D geometry. Periodic acquisition of volumetric data sets in the course of the experiment makes it possible to carry out a 4D analysis of the model, i.e. 3D analysis through time. Examples are shown of 4D analysis of analogue models that tested the influence of lateral rheological changes on the structures obtained in contractional and extensional settings.

Analogue models have been used since the 19th century to simulate various kinds of geological structures in nature. The main objective of analogue models is to create a geometric analogue of a natural structure. Early analogue model experiments include those of Hall (1815), Favre (1878), Daubrée (1879) and Cadell (1890). Experiments on horizontal shortening were conducted by Cadell (1890), who described folding and thrusting of a layered model consisting of sand and plaster of Paris (Fig. 1) and suggested similarities with structures in the Highlands of Scotland and the Alps.

Analogue modelling offers the opportunity to determine the relation between imposed boundary conditions and resulting structures. Specific controlling parameters can be varied in order to assess their importance for the structure being considered. In analogue models, materials are used whose rheological properties are assumed to be similar to those of rocks in nature, e.g. sand, clay, paraffin, wax or silicone. One major advantage of analogue model experiments is the ability to analyse progressive deformation, from the initial undeformed state to the final deformed state with a spatial and temporal resolution that is not possible in natural field examples. The experiments are especially meant to stimulate the conception of testable hypotheses regarding the development of natural deformation structures. Results of analogue modelling have been applied to both small and large-scale natural structures.

Analogue models have provided important new insights into the geometry and progressive evolution of geological structures. In some cases, experimental studies proved to be fundamental for understanding natural deformation structures. For example, using clay models, Riedel (1929), Cloos (1928, 1930) and later Tchalenko (1970) and Wilcox *et al.* (1973) proposed an explanation for fractures and faults associated with strike-slip faulting. Experiments on folding by Biot *et al.* (1961) and Ramberg (1964) revealed that fold wavelength is a function of relative viscosity and bed thickness. Experiments by McClay & Ellis (1987), Ellis & McClay (1988) and McClay (1990), documented in detail fundamental fault geometries and roll-over anticlines within the hanging walls of listric extensional fault systems. More recently, analogue modelling by Chemenda *et al.* (1995) revealed possible mechanisms for syn-collisional exhumation.

Until the late 1980s, analogue models were analysed either by recording the surface evolution, by monitoring the structures through transparent side panels (where undesirable boundary effects are largest), and/or by physically cutting a series of sections through the consolidated model. Such methods of analysis did not allow a full 3D reconstruction of the model at the end of

From: MEES, F., SWENNEN, R., VAN GEET, M. & JACOBS, P. (eds) 2003. *Applications of X-ray Computed Tomography in the Geosciences*. Geological Society, London, Special Publications, **215**, 213–223. 0305-8719/03/$15.

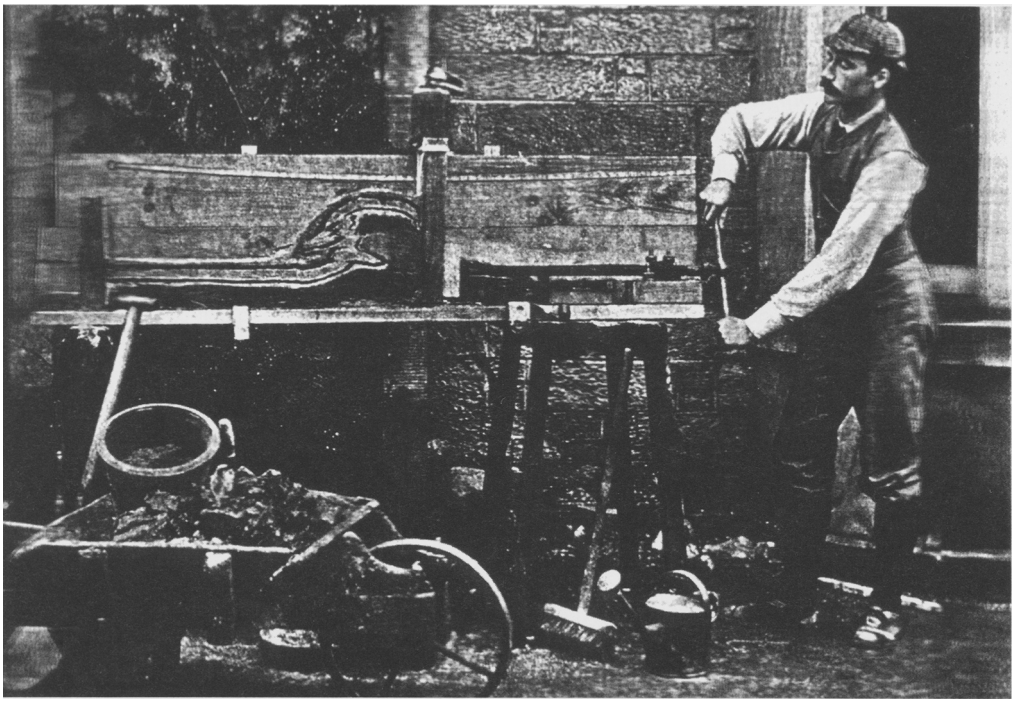

Fig. 1. Experimental modelling of mountain-building processes by Cadell (1890), who shortened an initially horizontally layered sequence consisting of plaster of Paris and sand to investigate thrusting and folding. Reproduced by permission of the Royal Society of Edinburgh.

the experiment, nor was it possible to study the internal geometry of the model in the course of the experiment. This was especially a disadvantage when analysing the geometry and evolution of non-cylindrical structures. X-ray computed tomography (CT) overcomes this disadvantage because this technique makes it possible to visualize the interior of an analogue model without destroying it.

X-ray computed tomography

X-ray CT generates cross-sectional slices through an analogue model and thus allows a detailed analysis of its internal geometry and kinematics. X-ray attenuation is mainly a function of material density, atomic number and thickness. Layering in the analogue model is produced by using analogue materials with different attenuation values. The number of cross-sectional slices that can be obtained for a particular stage in the evolution of the model depends mainly on the X-ray dose intensity needed for proper visualization and the performance of the X-ray source. The time between consecutive runs is dictated by the required cooling of this source below a certain threshold value. Because of the time involved in CT data acquisition and the long cooling duration of the X-ray source, early medical scanners could only record a limited number of cross-sectional slices. Another limiting factor was the computational capacity needed to calculate images from projectional raw data profiles. Periodic acquisition of sections at similar positions during deformation made it nevertheless possible to follow the 2D evolution of structures in time. However, the time-consuming recording of closely spaced sequential cross-sectional slices, necessary for a full 3D analysis of the model, was generally not carried out until the end of the experiment (e.g. Mandl 1988; Colletta *et al.* 1991; Philippe 1995; Schreurs & Colletta 1998).

X-ray CT has in the past been used to study structures resulting from shortening and oblique shortening (Colletta *et al.* 1991; Wilkerson *et al.* 1992; Philippe 1994; Guillier *et al.* 1995; Letouzey *et al.* 1995; Philippe 1995; Mugnier *et al.* 1997; Schreurs 1997; Philippe *et al.* 1998; Schreurs & Colletta 1998; Nieuwland *et al.* 2000; Schreurs

et al. 2001), extension and oblique extension (Mandl 1988; Naylor *et al.* 1994; Schreurs & Colletta 1998), strike-slip (Richard 1990; Schreurs 1994, 2003; Richard *et al.* 1995; Ueta *et al.* 2000), and inversion (Roure *et al.* 1992; Vially *et al.* 1994; Letouzey *et al.* 1995).

Recent technological improvements have resulted in more powerful X-ray CT scanners. The acquisition system of helical or spiral scanners (Fig. 2) revolves around the object as the object moves in the longitudinal direction, orthogonal to the scanning plane. In this manner, 3D volume raw data on analogue models are easily acquired. This technique makes it possible to calculate an almost unlimited number of closely spaced serial cross-sections retrospectively from the raw data. Data acquisition time for such a 3D data set depends on the X-ray dose necessary to adequately penetrate the analogue material (i.e. material composition and thickness), detector quality and the performance of the entire acquisition system (e.g. rotation time, table speed,

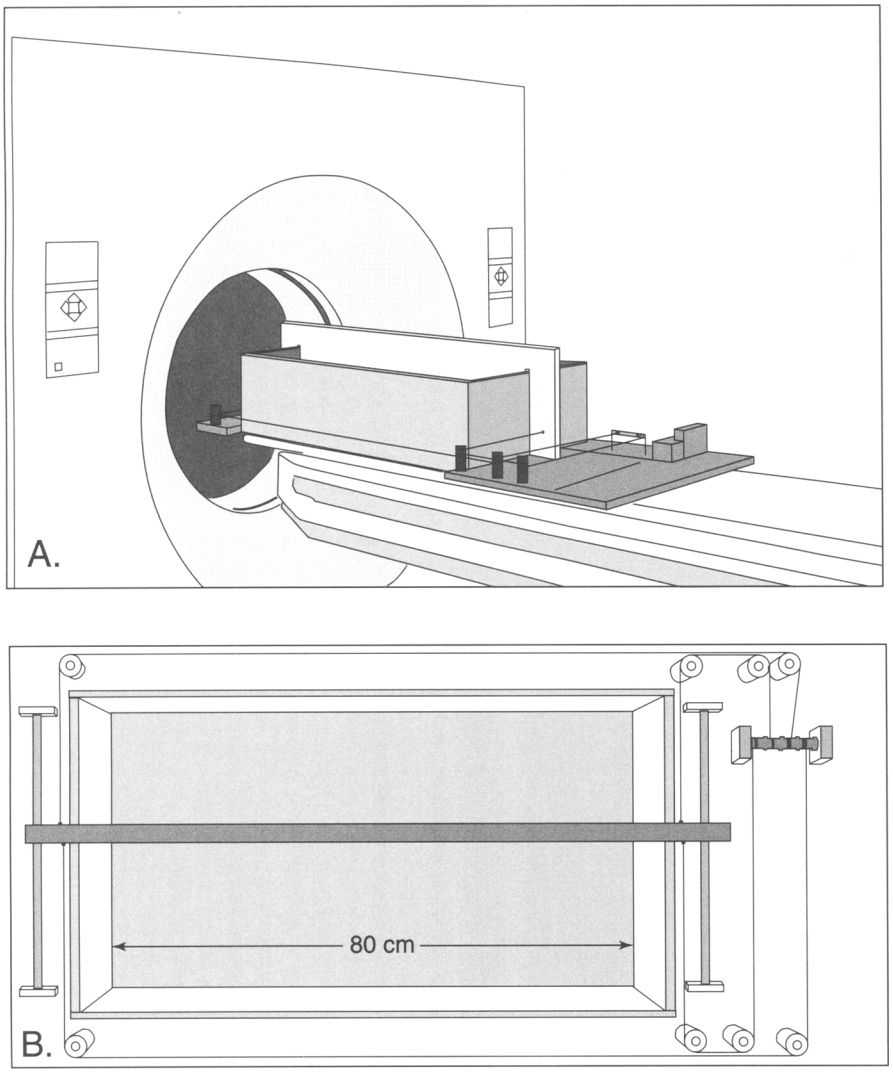

Fig. 2. (**a**) Helical X-ray CT scanner and experimental apparatus. During rotation of the acquisition system the experimental apparatus is translated horizontally through the field of investigation making it possible to obtain three-dimensional volume raw data. (**b**) Top view of experimental apparatus used to test the influence of the shape and position of viscous layers during shortening or extension of a brittle-viscous analogue model.

data transfer, computation speed). Slice spacing will only affect the post-processing time. Periodic acquisition of such volumetric data sets makes it possible to follow the 3D evolution of models from the initial undeformed stage to the final deformed stage. This opens new and exciting perspectives for a complete 4D analysis (3D through time) of analogue models (Schreurs *et al.* 2001). Using computer visualization software, the digital data also allow the reconstruction of any desired section, be it horizontal, vertical or oblique.

Experimental procedure

In normal gravity experiments, dry granular materials with low cohesion are commonly used as analogue materials for brittle rocks in the upper crust because they obey the Mohr-Coulomb criterion of failure. Viscous materials are generally used to simulate viscous flow of evaporites in the upper crust or rocks in the lower crust. X-ray attenuation values of different analogue materials were first determined by Colletta *et al.* (1991), who selected sand, glass powder and glass microbeads with an average grain size of about 100 μm for brittle modelling experiments. Attenuation values of granular materials depend mainly on mineral composition of the grains, on grain size and on compaction (Colletta *et al.* 1991).

X-ray attenuation values of several granular materials with grain sizes between 80 and 200 μm were tested for potential use in analogue modelling experiments (Table 1). Quartz sand (80–200 μm) and corundum sand ('Normalkorund', 80–125 μm) were selected as brittle analogue materials. The angles of internal friction of quartz and corundum sand are about 35° and 37°, respectively. These materials can be used to simulate upper crustal rocks that have comparable angles of internal friction at low normal stresses (Byerlee 1978). As viscous analogue material, polydimethyl-siloxane (PDMS) was used, which is a non-toxic, transparent material with a linear viscosity of 5×10^4 Pa·s at room temperature and at strain rates below 3×10^{-3} s^{-1} (Weijermars 1986). The different attenuation values for PDMS (70 Hounsfield Units, HU), quartz sand (870 HU) and corundum sand (1240 HU) make it possible to construct layered brittle and brittle-viscous models. Attenuation values of adjacent analogue materials should differ by at least 200 HU for optimal visualization of the boundaries between the two materials. During deformation of the model, faults develop in granular materials. Faults correspond to dilatant zones along which the grains have been perturbed. Dilatancy along faults results in a lower density and thus in a reduction of the attenuation compared to the surrounding unfaulted material. This contrast in attenuation makes faults clearly visible in CT images.

The experimental set-up includes a rectangular wooden box with a length of 80 cm, a width of 43 cm and a height of 17 cm (Fig. 2). A vertical mobile wall driven by a motor produces either extension or shortening. In contrast to wood, metal objects strongly attenuate X-rays and cause important artefacts in image computing.

Table 1. *Material parameters and distributors of analogue materials*

Material	Grain size (μm)	Density (g/cm^3)	Attenuation value (HU)	ϕ_{peak} (°)	Distributor
Air	–	0.0013	−1000	–	–
Water	–	1.0	0	–	–
Quartz sand	80–200	1.56*	870	35	(1)
Quartz sand (ref. BDF Gallardon 28)	~140	~1.45*	740	–	(2)
Corundum sand ('Edelkorund')	105–149	1.89*	1070	36	(1)
Corundum sand ('Normalkorund')	88–125	1.90*	1240	37	(1)
Glasspowder ('G2', ref. 585-10)	88–125	1.09*	360	36	(3)
Glasspowder (recycled glass, white)	100–210	1.24*	690	42	(1)
Glass microbeads	70–110	1.48*	950	22	(4)
Polydimethylsiloxane (GUM SGM 36)	–	0.96	70	–	(5)

Asterisk indicates that the material was sifted into a container before density measurement. Average attenuation values are in Hounsfield units (HU), measured with a Toshiba Asteion CT scanner, at 120 kV X-ray tube energy. ϕ_{peak} is the angle of internal peak friction, measured for all granular materials (except quartz sand, ref. BDF Gallardon 28) using a ring-shear tester. (1) www.carloag.ch; (2) Ets. Bervialle, 11 rue Teheran, F-75008 Paris; (3) V.R.C., rue des Tilleuls, F-95870 Bezons; (4) www.worf.de; (5) S.T.I./Dow Corning, 19 rue d'Arsonval, F-69680 Chassieu.

For this reason, the motor was placed adjacent to the wooden box. Analogue models were analysed by single- or multi-slice helical X-ray CT scanners. The Siemens Somatom Plus 4 single-slice helical scanner used a 120 kV voltage, a 130 mA current and 2 mm X-ray beam width to differentiate analogue material attenuation. Rotation time of source and detector was 1 s and table feed per rotation was 4.2 mm. During one rotation, the X-ray fan examines a slice of the object that is 2 mm thick. The diameter of the circular opening of the X-ray scanner was 55 cm, but the area of investigation is a circle 45 cm in diameter. In contrast to the single-slice scanner, the Toshiba Asteion multi-slice helical CT scanner investigates four slices through the model simultaneously during one rotation. Each slice has a selectable thickness between 0.5 and 8 mm. We used a 120 kV voltage, 100 mA current and 8 mm beam width. During one rotation, four 2 mm slices were examined. Rotation time was 1 s and table feed per rotation was 11 mm. The multi-slice scanner has a circular opening 50 cm in diameter, whereas the field of investigation is a circle 40 cm in diameter. There is no noticeable difference in image quality or resolution between the two instruments used. However, the advantage of the multi-slice CT is that this scanner allows the acquisition of a larger 3D volume raw data set during one scan.

Deformation of the analogue model takes place in the investigation field of the helical X-ray CT scanner. 3D volumetric data sets were acquired at regular time intervals in order to follow the 3D evolution of models from the initial undeformed stage to the final deformed stage. From the 3D volume raw data, cross-sectional slices with 2 mm spacing were retrospectively computed. Attenuation values were computed for a 512×512 matrix of volume elements (voxels). The computed values produce a 512×512 pixel grey-scale image. Digital image processing and computer visualization software allow the reconstruction of sections in any direction through a 3D data set and the production of movies that show, for example, successive serial cross-sections through one particular deformation stage or the temporal evolution of model deformation in 2D or 3D.

Using brittle-viscous analogue models, we investigated the influence of the shape and position of a viscous layer on the resulting structures during shortening and extension. In the shortening experiment, initial width of the model was 27 cm and its initial thickness was 3 cm. In the extension experiment, initial width and thickness were 22.5 cm and 3.5 cm, respectively. Very high width/thickness ratios should be avoided, as these result in poorly defined images, because image computation is optimized for objects with round cross-sections.

Modelling results

Influence of basal rheological changes during shortening

The experimental set-up for the shortening experiment is shown in Figure 3. A rectangular layer of viscous PDMS (simulating an evaporite layer), 40 cm long, 17 cm wide and 5 mm thick was placed on top of the wooden base next to the mobile wall. Alternating layers of quartz and corundum sand (simulating a sequence of competent sedimentary rocks) were poured on top.

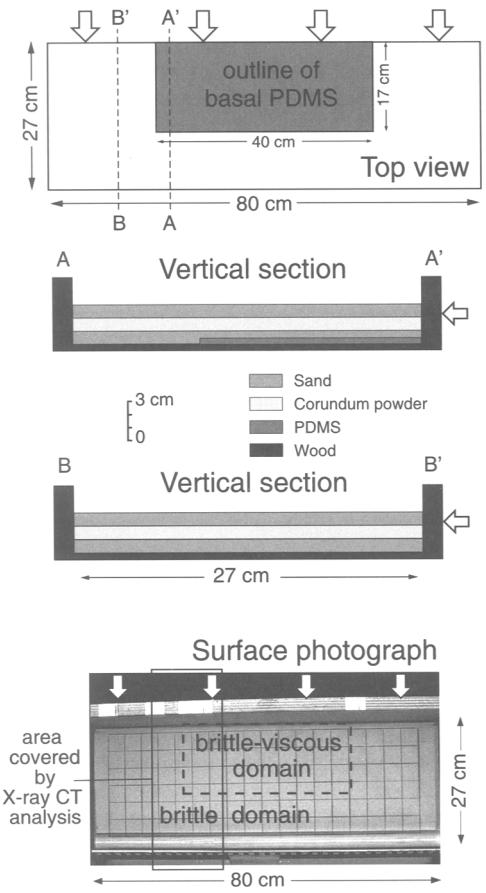

Fig. 3. Initial experimental set-up for testing the influence of basal rheological changes during shortening, illustrated by a top view, two vertical sections and surface photograph.

Purely for descriptive purposes, we refer to the domain containing the quartz-corundum-quartz sand layers as the brittle domain and to the domain with both quartz-corundum-quartz sand layers and a basal viscous PDMS layer as the brittle-viscous domain. Initially, the undeformed analogue model was 27 cm wide. By displacing the vertical mobile wall the model was shortened by 9 cm. CT 3D raw data acquisition was performed at the initial undeformed stage and at every full cm of progressive shortening.

There was a marked difference in structural evolution between the brittle and brittle-viscous domains (Fig. 4; Movies A-1 and A-2). In the brittle domain, thrust faults were closely spaced and a narrow and high fold-and-thrust belt formed. The sequence of thrusting propagated forward and the belt had a dominant vergence of thrusts and associated folds. In the brittle-viscous domain, however, the thrust belt was wider and lower, and there was no consistent vergence of thrusts and folding. A transfer zone formed in the transition zone between the brittle and brittle-viscous domains (Fig. 5; Movies A-3 and A-4). It linked thrusts that formed at different locations and stages in the evolution of the model. The transfer zone rooted in the viscous layer and its surface strike was parallel to the orientation of the boundary between viscous and brittle material at depth, and parallel to the shortening direction. The dip of the transfer zone was shallow (<30°) and the angle of dip changed along strike (Fig. 6; Movie A-5). Forward thrusting in the brittle domain propagated along strike into the brittle-viscous domain and resulted in out-of-sequence thrusts in the latter domain. Back thrusts forming above the basal PDMS interfere with forward thrusts that developed in the purely brittle domain. These laterally propagating forward and backward thrusts contributed to the complexity of the fault pattern (Movie A-6). The experiments suggest that location and orientation of transfer zones in nature may be controlled by basal rheological changes.

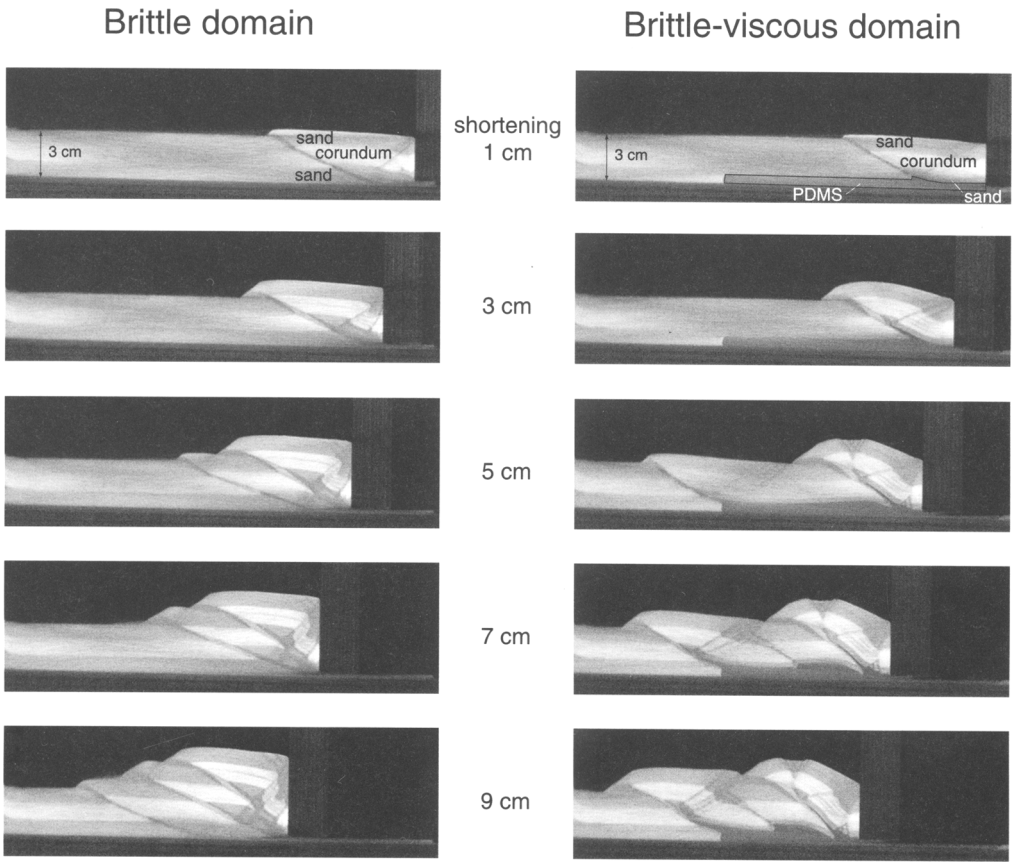

Fig. 4. Comparison of structural evolution between brittle and brittle-viscous domains for the shortening experiment by successive transverse computed X-ray CT images of the progressively deformed model.

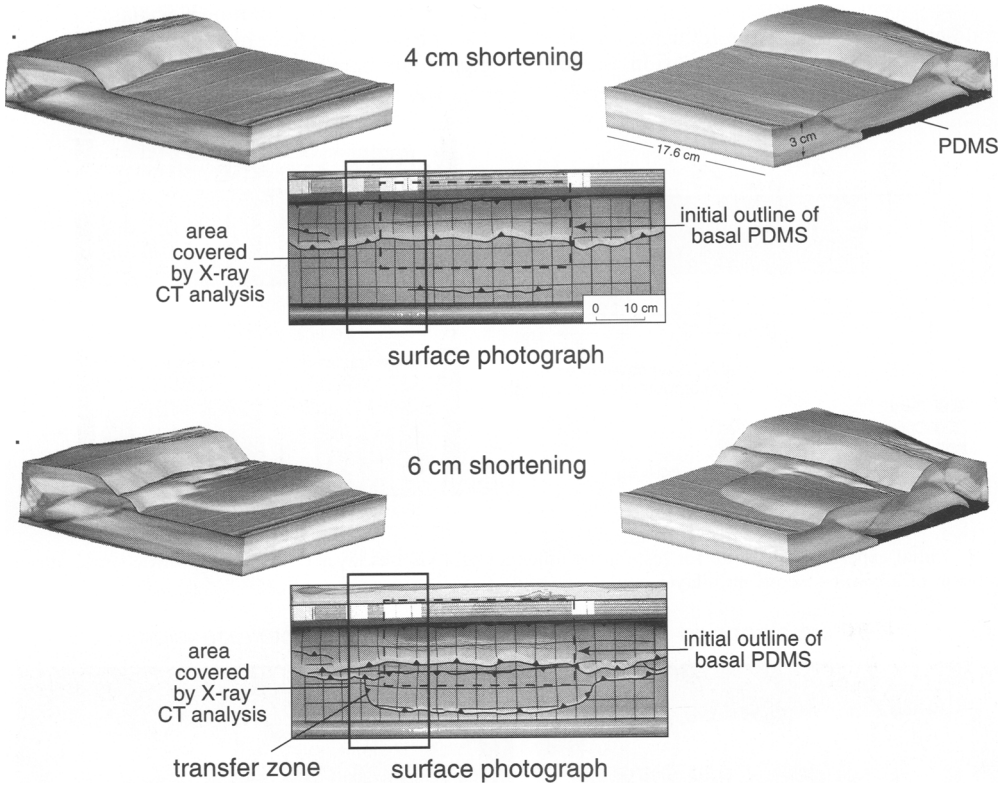

Fig. 5. Surface photograph with superposed interpretation and two oblique 3D views, shown for two consecutive stages of the shortening experiment, illustrating the development of a transfer zone, at 4 cm shortening (**a**) and 6 cm shortening (**b**). The rectangle indicates the area of three-dimensional analysis of one particular stage. The dashed rectangle indicates the initial outline of the basal viscous silicone.

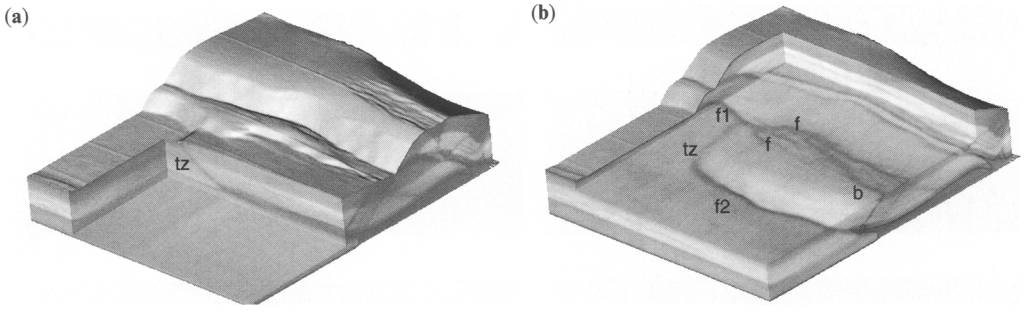

Fig. 6. Two three-dimensional views of an analogue model at 6 cm shortening. (**a**) Longitudinal section (perpendicular to shortening direction) showing a shallow dip angle of the transfer zone (lateral ramp). (**b**) Horizontal section showing the position of the transfer zone, which connects the frontal ramp in the brittle domain, (f1), with the frontal ramp in the brittle-viscous domain, (f2); back thrusts in brittle-viscous domain disappear laterally or interfere with forward thrusts that originated in the brittle domain and propagated sideways into the brittle-viscous domain; tz = transfer zone (lateral ramp); f = forward directed thrust; b = back thrust.

Influence of lateral rheological changes during extension

Analogue modelling on the influence of lateral rheological changes during extension was done with the experimental set-up shown in Figure 7. The base of the rectangular wooden box is overlain by an alternation of nine plexiglass bars (each bar is 5 mm wide, 5 cm high and 80 cm long) and eight foam bars (each bar is 3 cm wide, 5 cm high

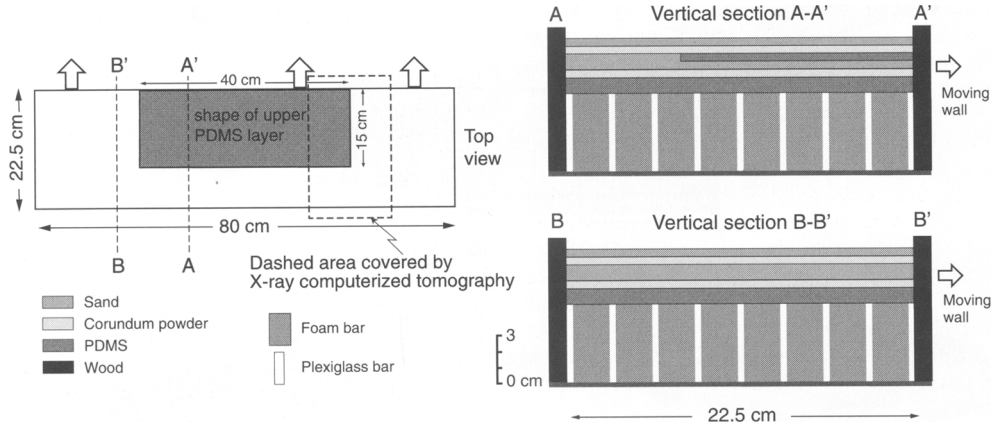

Fig. 7. Initial experimental set-up for testing the influence of a viscous layer embedded in brittle strata during extension of a brittle-viscous multilayer model.

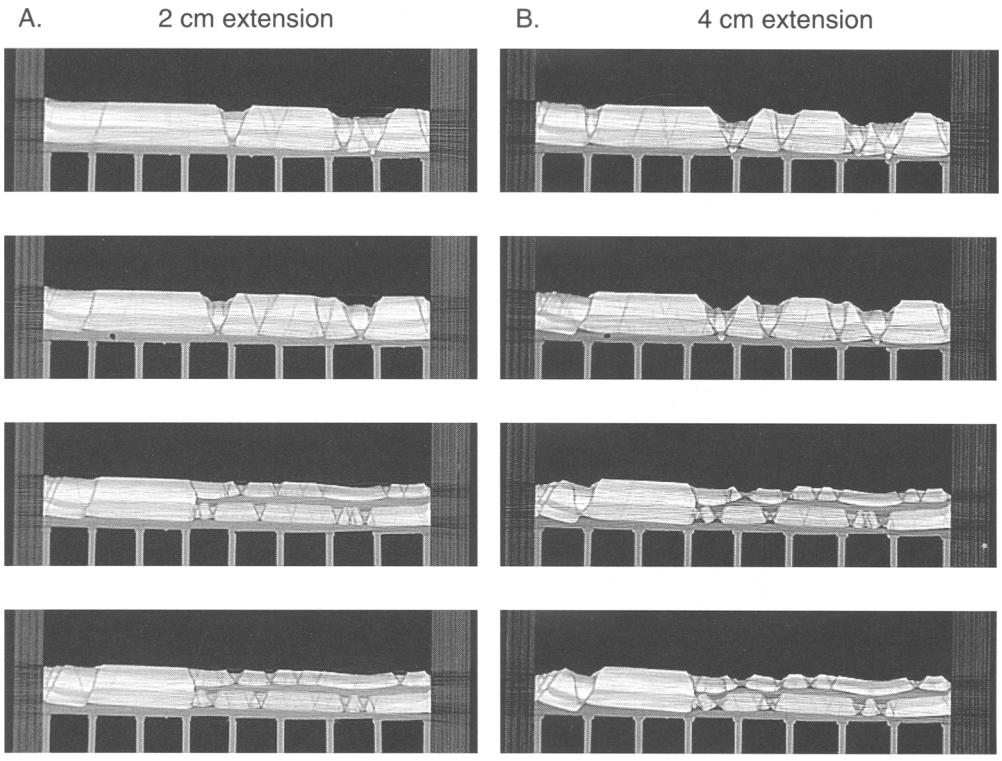

Fig. 8. Vertical sections through the brittle-viscous multilayer model at 2 cm extension, (**A**), and 4 cm extension, (**B**). The upper two sections are taken from the domain with only a basal viscous layer; the lower two sections are taken from the domain with two viscous layers. Note that the presence of a second viscous layer caused the development of decoupled conjugate normal fault systems in the upper and lower brittle compartments.

and 80 cm long). Before constructing the stratified brittle-viscous analogue model, the assemblage of plexiglass and foam bars was shortened by 6 cm. In the shortened state, the width of each foam bar was reduced to circa 2.25 cm, whereas the width of the plexiglass bars remained unchanged. The brittle-viscous multilayer model was then constructed on top of the shortened assemblage and consisted of a 1 cm thick basal viscous layer and an upper, smaller viscous layer embedded in brittle strata made up of corundum and quartz sand (Fig. 7). The upper viscous layer was placed near the extending mobile wall and covered only part of the underlying brittle layers. The presence of foam bars alternating with plexiglass bars in combination with the overlying basal viscous layer prevented localization of deformation near the extending mobile wall. The initial width of the model was 22.5 cm and total extension was 5 cm. During extension, the foam bars 'decompressed' and deformation in the model was distributed over the width of the model. CT 3D raw data were acquired of the initial undeformed stage and at every 5 mm of progressive extension.

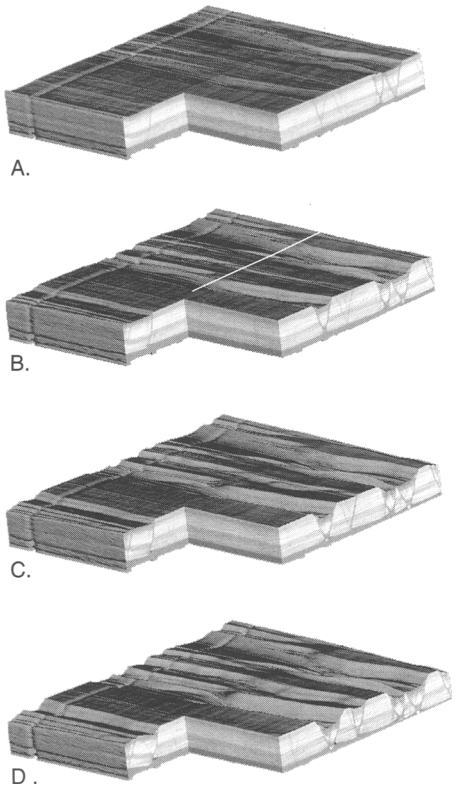

Fig. 9. Progressive evolution of structures at 1 cm (**a**), 2 cm (**b**), 3 cm (**c**) and 4 cm (**d**) extension, illustrated by 3D views. The white line in (**b**) indicates the position of the extensional transfer zone. The discontinuity near the left-hand side of each block results from missing cross-sections.

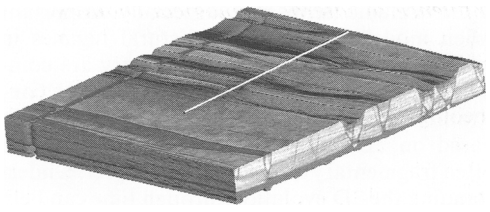

Fig. 10. Horizontal section through a 3D view of the analogue model at 4 cm extension. The location of the extensional transfer zone (indicated by a white line) is directly linked to the lateral termination of the interbedded viscous layer.

The shape and position of the upper viscous layer had a profound influence on the structural style that developed in the course of the experiment. The upper viscous layer embedded within brittle strata initially caused the development of two independent, decoupled conjugate normal fault systems in upper and lower brittle compartments (Fig. 8; Movies B-1 and B-2). The width between conjugate normal faults reflects the depth to detachment (viscous layer). In the part of the model where there was only one basal viscous layer, the width between conjugate faults was large, whereas in the part of the model with a second viscous layer embedded in brittle layers, this width was small (Fig. 9; Movie B-3). The location and orientation of extensional transfer zones, visible in horizontal sections (Fig. 10; Movie B-4) and in surface view, was directly linked to the geometry of the interbedded viscous layer. These transfer zones connect widely spaced conjugate normal fault systems with less widely spaced systems.

Concluding remarks

This paper shows the great potential of CT scanning for a complete analysis of analogue models. The 3D volumetric raw data allow the computation of contiguous cross-sectional slices parallel to the transport direction. Computer visualization software makes it possible to reconstruct the analogue model in three dimensions and to reconstruct sections in any direction. On the basis of 3D reconstructions, animations can be created in order to study the spatial evolution of structures at a specific stage, or to study the 4D evolution of the model.

CT volume scans are especially important when modelling complex structural regimes in which lateral changes in 3D geometry are common. 3D imaging of models can provide constraints for interpretations of complex zones based on 2D and 3D seismic data, which are often fragmentary or difficult to interpret. Understanding the 3D evolution through time can help geologists and seismic interpreters in developing kinematic models.

The experiments suggest that the position and orientation of transfer zones in nature might be directly linked to initial lateral rheological changes within a layered sequence. Basal rheological changes in the shortening experiment resulted in shallowly dipping transfer zones (lateral ramps) that root directly at the lateral contact between viscous and brittle layer. In the extensional experiment, vertical transfer zones formed directly above the lateral boundary between upper viscous layer and adjacent brittle layers.

Movies

Ten short movies on the accompanying CD-ROM (back cover of this Special Publication) illustrate the structural evolution of the shortening and extension experiment. For more details see text file on CD-ROM.

Funding by Hochschulstiftung Bern and Swiss National Science Foundation Grant 2000-0554.11 98/1 is gratefully acknowledged. The manuscript benefited from constructive reviews by M. Sintubin and A. Vervoort. H.-P. Bärtschi is thanked for technical assistance, A. Schneider and C. Seiler for assistance in CT data acquisition, and J. Lohrmann, N. Kukowski and O. Oncken for allowing M. Panien to use the ring-shear tester at the GeoForschungsZentrum in Potsdam to measure mechanical parameters of our granular analogue materials.

References

BIOT, M.A., ODÉ, H. & ROEVER, W.L. 1961. Experimental verification of the theory of folding of stratified viscoelastic media. *Geological Society of America Bulletin*, **72**, 1621–1632.

BYERLEE, J.D. 1978. Friction of rocks. *Pure Applied Geophysics*, **116**, 97–115.

CADELL, H.M. 1890. Experimental researches in mountain building. *Transactions of the Royal Society of Edinburgh*, **35**, 337–357.

CHEMENDA, A.I., MATTAUER, M., MALAVIEILLE, J. & BOKUN, A.N. 1995. A mechanism for syn-collisional rock exhumation and associated normal faulting: Results from physical modelling. *Earth and Planetary Science Letters*, **132**, 225–232.

CLOOS, H. 1928. Experimente zur inneren Tektonik. *Zentralblatt für Mineralogie, Geologie und Paläontologie*, **12**, 609–621.

CLOOS, H. 1930. Zur experimentellen Tektonik V. Vergleichende Analyse dreier Verschiebungen. *Geologische Rundschau*, **21**, 353–367.

COLLETTA, B., BALE, P., BALLARD, J.F., LETOUZEY, J. & PINEDO, R. 1991. Computerized X-ray tomography analysis of sandbox models: examples of thin-skinned thrust systems, *Geology*, **19**, 1063–1067.

DAUBRÉE, A. 1879. *Etude synthétique de géologie expérimentale*. Dunod, Paris.

ELLIS, P.G. & MCCLAY, K.R. 1988. Listric extensional fault systems. Results of analogue model experiments. *Basin Research*, **1**, 55–70.

FAVRE, A. 1878. The formation of mountains. *Nature*, **19**, 103–106.

GUILLIER, B., BABY, P., COLLETTA, B., MENDEZ, E., LIMACHI, R., LETOUZEY, J. & SPECHT, M. 1995. Analyse géometrique et cinématique d'un 'duplex' issu d'un modèle analogique visualisé en 3D par tomographie aux rayons X. *Comptes Rendus de l'Academie des Sciences, Serie II*, **321**, 901–908.

HALL, J. 1815. On the vertical position and convolution of certain strata and their relation with granite. *Transactions of the Royal Society of Edinburgh*, **7**, 79–108.

LETOUZEY, J., COLLETTA, B., VIALLY, R. & CHERMETTE, J.C. 1995. Evolution of salt-related structures in compressional settings. *In*: JACKSON, M.P.A., ROBERTS, D.G. & SNELSON, S. (eds) *Salt Tectonics: A Global Perspective*. American Association Petroleum Geologists Memoir, **65**, 41–60.

MANDL, G. 1988. *Mechanics of Tectonic Faulting: Models and Basic Concepts*. Elsevier, Amsterdam.

MCCLAY, K.R. 1990. Extensional fault systems in sedimentary basins: a review of analogue model studies. *Marine and Petroleum Geology*, **7**, 206–233.

MCCLAY, K.R. & ELLIS, P.G. 1987. Geometries of extensional fault systems developed in model experiments. *Geology*, **15**, 341–344.

MUGNIER, J.L., BABY, P., COLLETTA, B., VINOUR, B., BALE, P. & LETURMY, P. 1997. Thrust geometry controlled by erosion and sedimentation: a view from analogue models, *Geology*, **25**, 427–430.

NAYLOR, M.A., LARROQUE, J.M. & GAUTHIER, B.D.M. 1994. Understanding extensional tectonics: insights from sandbox models. *In*: ROURE, F. (ed.) *Geodynamic Evolution of Sedimentary Basins*. Editions Technip, Paris, 69–83.

NIEUWLAND, D.A., LEUTSCHER, J.H. & GAST, J. 2000. Wedge equilibrium in fold-and-thrust belts: prediction of out-of-sequence thrusting based on sandbox experiments and natural examples. *Geologie en Mijnbouw, Netherlands Journal of Geosciences*, **79**, 81–91.

PHILIPPE, Y. 1994. Transfer zone in the southern Jura thrust belt (eastern France): geometry, development and comparison with analogue modelling experiments. *In*: MASCLE, A. (ed.) *Hydrocarbon and Petroleum Geology of France*. European Association of Petroleum Geologists, **4**, 327–346.

PHILIPPE, Y. 1995. *Rampes Latérales et Zones de Transfert dans les Chaînes Plissées: Géometrie, Conditions de Formations et Pièges Structuraux Associés*. PhD thesis, Université de Savoie.

PHILIPPE, Y., DEVILLE, E. & MASCLE, A. 1998. Thin-skinned inversion tectonics at oblique basin margins: example of the western Vercors and Chartreuse Subalpine massifs (SE France). *In*: MASCLE, A., PUIGDEFÀBREGAS, C., LUTERBACHER, H.P. & FERNANDEZ, M. (eds) *Cenozoic Foreland Basins of Western Europe*. Geological Society, London, Special Publications, **134**, 239–262.

RAMBERG, H. 1964. Selective buckling of composite layers with contrasted rheological properties: a theory of simultaneous formation of several orders of folds. *Tectonophysics*, **1**, 307–341.

RICHARD, P. 1990. Champs de failles au dessus d'un décrochement de socle: modélisation expérimentale. *Mémoires et Documents du Centre Armoricain d'Etude Structurale des Socles*, **34**.

RICHARD, P., NAYLOR, M.A. & KOOPMAN, A. 1995. Experimental models of strike-slip tectonics, *Petroleum Geoscience*, **1**, 71–80.

RIEDEL, W. 1929. Zur Mechanik geologischer Brucherscheinungen. *Zentralblatt für Mineralogie, Abteilung B*, 354–368.

ROURE, F., BRUN, J.P., COLLETTA, B. & VAN DEN DRIESSCHE, J. 1992. Geometry and kinematics of extensional structures in the Alpine Foreland Basin of southeastern France. *Journal of Structural Geology*, **14**, 503–519.

SCHREURS, G. 1994. Experiments on strike-slip faulting and block rotation. *Geology*, **22**, 567–570.

SCHREURS, G. 1997. Experiments on faulting in zones of oblique shortening. *The Leading Edge*, 1159–1163.

SCHREURS, G. 2003. Fault development and interaction in distributed strike-slip shear zones: an experimental approach. *In*: STORTI, F., HOLDSWORTH, R.E. & SALVINI, F. (eds) *Intraplate Strike-slip Deformation Belts*. Geological Society, London, Special Publications, **210**, 35–52.

SCHREURS, G. & COLLETTA, B. 1998. Analogue modelling of faulting in zones of continental transpression and transtension. *In*: HOLDSWORTH, R.E., STRACHAN, R.A. & DEWEY, J.F. (eds) *Continental Transpressional and Transtensional Tectonics*. Geological Society, London, Special Publications, **135**, 59–79.

SCHREURS, G., HÄNNI, R. & VOCK, P. 2001. 4-D Analysis of analog models: experiments on transfer zones in fold-and-thrust belts. *In*: KOYI, H.A. & MANCKTELOW, N.S. (eds) *Tectonic Modeling: A Volume in Honor of Hans Ramberg*. Geological Society of America Memoir, **193**, 179–190.

TCHALENKO, J.S. 1970. Similarities between shear zones of different magnitudes. *Geological Society of America Bulletin*, **81**, 1625–1640.

UETA, K., TANI, K. & KATO, T. 2000. Computerized X-ray tomography analysis of three-dimensional fault geometries in basement-induced wrench faulting. *Engineering Geology*, **56**, 197–210.

VIALLY, R., LETOUZEY, J., BÉNARD, F., HADDADI, N., DESFORGES, G., ASKRI, H. & BOUDJEMA, A. 1994. Basin inversion along the North African margin of the Saharan Atlas (Algeria). *In*: ROURE, F. (ed.) *Peri-Tethyan Platforms*. Editions Technip, Paris, 79–118.

WEIJERMARS, R. 1986. Flow behaviour and physical chemistry of bouncing putties and related polymers in view of tectonic laboratory applications. *Tectonophysics*, **124**, 325–358.

WILCOX, R.E., HARDING, T.E. & SEELY, D.R. 1973. Basic wrench tectonics. *American Association of Petroleum Geologists Bulletin*, **57**, 74–96.

WILKERSON, M.S., MARSHAK, S. & BOSWORTH, W. 1992. Computerized tomographic analysis of displacement trajectories and three-dimensional fold geometry above oblique thrust ramps. *Geology*, **20**, 439–442.